CRYSTAL GROWTH & DESIGN

Article

Cite This: Cryst. Growth Des. XXXX, XXX, XXX−XXX

pubs.acs.org/crystal

Crystal Growth and Magnetic Properties of $Pr_3Co_{2+x}Ge_7$ and the Sn-Stabilized $Ln_3Co_{2+x}Ge_{7-y}Sn_y$ (Ln = Pr, Nd, Sm)

Mojammel A. Khan,[‡,§] Gregory T. McCandless,[†] Katherine A. Benavides,[†] Thomas J. Martin,[†] Adzuira M. Palacios,[†] Anthony W. B. Samuel,[†] David P. Young,[‡] and Julia Y. Chan*[,†]

[†]Department of Chemistry and Biochemistry, The University of Texas at Dallas, 800 W. Campbell Road, Richardson, Texas 75080, United States

[‡]Department of Physics and Astronomy, Louisiana State University, Baton Rouge, Louisiana 70803, United States

Supporting Information

ABSTRACT: Single crystals of the ternary $Pr_3Co_{2+x}Ge_7$ and $Ln_3Co_{2+x}Ge_{7-y}Sn_y$ (Ln = Pr, Nd, Sm) adopting a disordered version of the $La_3Co_2Sn_7$ structure type have been prepared via flux-growth methods and characterized by single crystal X-ray diffraction. The structure consists of two lanthanide crystallographic sites with one occupying a cuboctahedral coordination environment and a second in a trigonal prismatic environment. The structure can also be described as an intergrowth of $AuCu_3$ and $CeNiSi_2$ structure types, and the stability of the germanide analogues requires Sn incorporation and Co site preferences. Magnetic properties of the $Pr_3Co_{2+x}Ge_{7-y}Sn_y$ series are highlighted with the Sn-substituted $Pr_3Co_{2.514(5)}Ge_{6.66(7)}Sn_{0.360(2)}$ orders magnetically near 5.8 K, while the germanide $Pr_3Co_{2.3376(5)}Ge_{7.056(7)}$ exhibits magnetic transitions at 5.3 and 9.3 K, arising from the magnetic sublattices with field-dependent magnetization revealing three metamagnetic transitions at 0.46, 0.80, and 2.1 T.

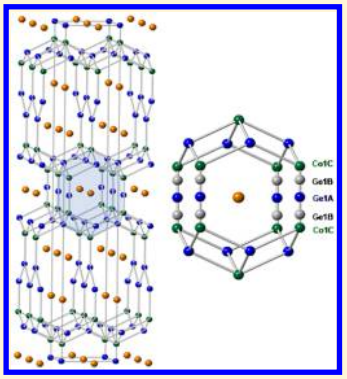

1. INTRODUCTION

The single crystalline growth of lanthanide based magnetic intermetallics has garnered much interest in the last two decades, primarily due to their unusual magnetic and electrical properties, such as valence fluctuations and magnetically mediated superconductivity.[1,2] As part of our efforts to understand the structural stability of the $Yb_3Rh_4Sn_{13}$ structure type,[3] we have determined that early lanthanides, such as $Ce_3Co_4Sn_{13}$,[4] can be stabilized for the stannides, while germanides can be prepared only with latter lanthanides such as $Lu_3Co_4Ge_{13}$.[5,6] While exploring the Ln-Co-Sn (Ln = lanthanides) phase space with substructural units of targeted intermetallics, we have focused on the orthorhombic $La_3Co_2Sn_7$ structure type for our study. $La_3Co_2Sn_7$ crystallizes in the space group *Cmmm* with cell dimensions of $a \sim 4.59$ Å × $b \sim 27.6$ Å × $c \sim 4.60$ Å.[7] The structure type is composed of one lanthanide in a cuboctahedral coordination environment (2*d* site) and a second (4*i* site) in a trigonal prismatic environment forming an intergrowth of $AuCu_3$ and $CeNiSi_2$ type subunits. The structure also consists of one transition metal site (4*j*) and four sites occupied by a Group 14 element.

The magnetic and electrical properties of several Ni analogues have been reported, including $Ce_3Ni_2Sn_7$,[8−10] and detailed studies on oriented crystals show that magnetic transitions are highly dependent on Ni concentration and magnetic fields. $Ln_3Ni_{2-x}Sn_7$ (Ln = La, Ce, Pr, and Nd) are highly anisotropic, and metamagnetic transitions were found for the $Ce_3Ni_{1.69}Sn_7$ and $Pr_3Ni_{1.56}Sn_7$ analogues. Another related structure is the $Ce_3Ni_{2+x}Si_{8-x}$ ($x \sim 1$) phase, which not only has Ni on the 4*j* site but also has Ni mixed on one of the Si sites (4*i*) in the asymmetric unit.[11] However, relatively few Co analogues have been reported. More recently, polycrystalline $Ce_3Co_2Sn_7$ was shown to behave similarly to the Ni compound, where the Ce located at the 4*i* site has a well-localized magnetic moment and increasing magnetic fields lead to lowering of the antiferromagnetic ordering temperature[12] along with a second Ce site being nonmagnetic or valence fluctuating.[13] In $U_3Co_2Ge_7$, two magnetic transitions were observed near 40 and 20 K that have been attributed to a ferromagnetic state and a spin reorientation, respectively, and the field-dependent magnetization shows a stepwise increase in the magnetization below 2 K. To study the structural stability of Co containing compounds adopting the $La_3Co_2Sn_7$ structure type, we present the crystal growth, structural characterization, and magnetic properties of $Ln_3Co_{2+x}Ge_{8-y}Sn_y$ (Ln = Pr, Nd, Sm). In this paper, we highlight the Pr analogues $Pr_3Co_{2.3376(5)}Ge_{7.056(7)}$ and $Pr_3Co_{2.514(5)}Ge_{6.66(7)}Sn_{0.360(2)}$.

2. EXPERIMENTAL SECTION

2.1. Synthesis. Samples of $Ln_3Co_{2+x}Ge_{7-y}Sn_y$ (Ln = Pr, Nd, Sm) were synthesized by arc-melting stoichiometric amounts of Ln, Co, and Ge pieces (3:2:7, all ≥99.9 wt % purity, metal basis) in an Ar atmosphere. Each button was arc-melted and flipped four times to ensure homogeneity. The buttons were then ground into a fine powder and combined with Sn in a 1:20 (Ln:Sn) ratio in a Canfield crucible

Received: June 6, 2018
Revised: July 29, 2018
Published: August 13, 2018

DOI: 10.1021/acs.cgd.8b00868
Cryst. Growth Des. XXXX, XXX, XXX−XXX

Table 1. Crystal Data, Data Collection, and Refinement Parameters

Crystal Data		
formula	$Pr_3Co_{2.3376(5)}Ge_{7.056(7)}$	$Pr_3Co_{2.514(5)}Ge_{6.66(7)}Sn_{0.360(2)}$
space group	*Cmmm*	*Cmmm*
a (Å)	4.2275(14)	4.2589(11)
b (Å)	25.911(8)	26.104(10)
c (Å)	4.2745(12)	4.3017(11)
V (Å^3)	468.2(2)	478.2(3)
Z	2	2
Data Collection		
cryst size (mm^3)	0.01 × 0.02 × 0.14	0.01 × 0.06 × 0.10
temperature (K)	298(2)	298(2)
θ (deg)	3.2−31.5	3.1−36.5
μ (mm^{-1})	41.59	40.63
collected reflns	5209	8376
unique reflns	499	723
Refinement		
reflns/param	499/35	723/35
R_{int}	0.048	0.042
h	$-6 \le h \le 6$	$-6 \le h \le 7$
k	$-38 \le k \le 36$	$-43 \le k \le 43$
l	$-6 \le l \le 5$	$-7 \le l \le 6$
$\Delta\rho_{max}$ (e Å^{-3})	4.56	1.06
$\Delta\rho_{min}$ (e Å^{-3})	−2.05	−2.82
GoF	1.02	1.14
extinction coeff	0.0007(2)	0.00158(7)
$R_1[F^2 > 2\sigma(F^2)]$	0.031	0.024
wR_2 (F^2)	0.085	0.041

Table 2. Fractional Atomic Coordinates and Equivalent Isotropic Displacement Parameters

	Wyckoff site	x	y	z	occupancy	U_{eq} (Å^2)[a]
$Pr_3Co_{2.3376(5)}Ge_{7.056(7)}$						
Pr1	2*c* (*mmm*)	1/2	0	1/2	1	0.0062(2)
Pr2	4*i* (*m*2*m*)	0	0.18393(2)	0	1	0.00508(19)
Co1	4*j* (*m*2*m*)	0	0.36944(5)	1/2	0.987(4)	0.0074(3)
Ge1A	2*a* (*mmm*)	0	0	0	0.544(3)	0.0227(10)
Ge1B	4*i* (*m*2*m*)	0	0.0293(3)	0	0.256(3)	0.0227(10)
Co1C	4*i* (*m*2*m*)	0	0.0520(4)	0	0.200(3)	0.0227(10)
Ge2	4*i* (*m*2*m*)	0	0.40894(5)	0	1	0.0109(3)
Ge3	4*j* (*m*2*m*)	0	0.09112(4)	1/2	1	0.0111(3)
Ge4A	4*j* (*m*2*m*)	0	0.27912(6)	1/2	0.987(4)	0.0060(4)
Ge4B	4*j* (*m*2*m*)	0	0.288(8)	1/2	0.013(4)	0.0060(4)
$Pr_3Co_{2.514(5)}Ge_{6.66(7)}Sn_{0.360(2)}$						
Pr1	2*c*	1/2	0	1/2	1	0.01081(12)
Pr2	4*i*	0	0.1845(2)	0	1	0.00704(9)
Co1	4*j*	0	0.36864(4)	1/2	0.950(5)	0.0081(3)
Sn1A	2*a*	0	0	0	0.360(2)	0.0164(3)
Ge1B	4*i*	0	0.03082(14)	0	0.333(2)	0.0164(3)
Co1C	4*i*	0	0.05473(19)	0	0.307(2)	0.0164(3)
Ge2	4*i*	0	0.40759(3)	0	1	0.00969(15)
Ge3	4*j*	0	0.09270(3)	1/2	0.948(5)	0.00985(15)
Ge4A	4*j*	0	0.27897(5)	1/2	1	0.00659(18)
Ge4B	4*j*	0	0.2908(8)	1/2	0.052(5)	0.00659(18)

[a] U_{eq} is defined as one-third of the trace of the orthogonalized U_{ij} tensor.

set.[14] The reaction was then backfilled with Ar (∼0.2 atm) and sealed in a fused-silica tube. The sealed reaction tube was then heated to 1175 °C at 100 °C/h, dwelled for 24 h, cooled to 815 °C at 3 °C/h, and centrifuged to remove excess Sn. The phases were etched with 3 M HCl, and single crystals of $Ln_3Co_{2+x}Ge_{7-y}Sn_y$ up to ∼1 mm in length were mechanically extracted.

Single crystals of $Pr_3Co_{2.3376(5)}Ge_{7.056(7)}$ were grown successfully with In flux (instead of Sn). Similar to the synthesis with Sn flux, the reactions with In flux were heated to 1175 °C at a rate of 100 °C/h, then slow cooled to 815 °C at a rate of 3 °C/h before centrifuging the excess In flux. The silver, metallic plate-shaped crystals were up to ∼1 mm in length. For completeness, a polycrystalline ingot of $Pr_3Co_2Sn_7$ was synthesized via arc-melting as previously described above, followed

DOI: 10.1021/acs.cgd.8b00868
Cryst. Growth Des. XXXX, XXX, XXX−XXX

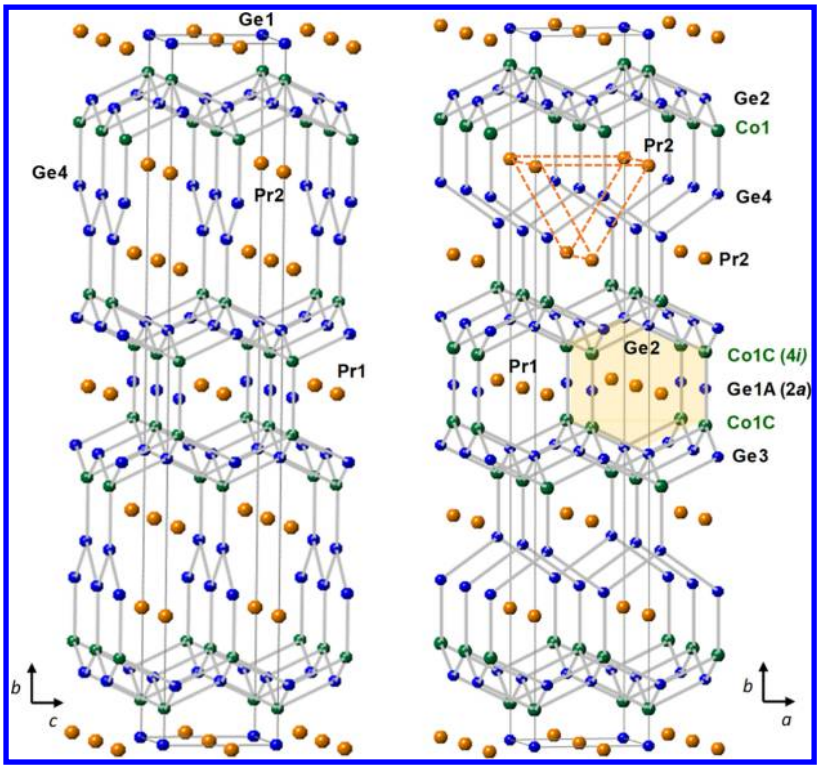

Figure 1. Crystal structure of $Pr_3Co_2Ge_7$ shown down the *a*-direction (left) and down the *c*-direction (right). Ge1b atoms are not shown for clarity.

with annealing at 850 °C for 7 days. Homogeneity of the polycrystalline ingot was determined using powder X-ray diffraction.

Attempts to synthesize La analogues, such as $La_3Co_2Ge_7$ or $La_3Co_2Ge_{7-x}Sn_x$, using either Bi, In, or Sn flux, consistently led to single crystalline $LaCoGe_3$.[15] Bi flux was also attempted for the growth of $Pr_3Co_2Ge_7$, but was unsuccessful and led to the synthesis of $Pr_2Co_3Ge_5$. While the single crystalline growth of germanides has been known to be successful using excess In flux,[16] attempts to grow single crystals of $Ln_3Co_{2+x}Ge_7$ (Ln = Nd and Sm) led to the stable formation of $LnCoGe_2$ (Ln = Nd, Sm). Growths were attempted for $Gd_3Co_2X_7$ (X = Ge, Sn), but the resulting products were $Gd_3Co_4Ge_{13}$ and $GdCoSn_2$, respectively. We speculate that Gd or smaller lanthanides are not stable in this structure type; however, the stability of competing phases makes it difficult to isolate $Ln_3Co_2Ge_7$ via flux-growth methods. For this reason, we did not attempt any syntheses with lanthanide elements beyond Gd.

2.2. Structure Determination. Powder X-ray diffraction was used to determine the homogeneity and phase purity of samples and was performed using a Bruker D8 Advance powder X-ray diffractometer operating at 40 kV/30 mA with a Cu Kα radiation (λ = 1.54184 Å). Single crystal X-ray diffraction data were collected on a Bruker D8 Quest Kappa single crystal X-ray diffractometer operating at 50 kV and 1 mA equipped with an IμS microfocus source (Mo Kα, λ = 0.71073 Å), a HELIOS optics monochromator, and a CMOS detector. The Bruker SAINT program was used to integrate the diffraction data while the absorption correction was performed using the Bruker program SADABS 2016/2 (multiscan method).[17] The crystal structures of $Ln_3Co_{2+x}Ge_{7-y}Sn_y$ (Ln = Pr, Nd, Sm) and $Pr_3Co_{2+x}Ge_7$ were solved using intrinsic phasing methods in SHELXT,[18] and anisotropically refined using SHELXL2014.[19] The data collection and refinement parameters are presented in Table 1, and the atomic positions for $Pr_3Co_{2+x}Ge_7$ and $Pr_3Co_{2+x}Ge_{7-y}Sn_y$ are presented in Table 2. The atomic positions for the Nd and Sm analogues are provided in the Supporting Information. For clarity throughout the paper, we will denote the composition of $Pr_3Co_{2.3376(5)}Ge_{7.056(7)}$ as $Pr_3Co_{2+x}Ge_7$ and $Pr_3Co_{2.514(5)}Ge_{6.66(7)}Sn_{0.360(2)}$ as $Pr_3Co_{2+x}Ge_{7-y}Sn_y$. The data have been assigned to the following deposition numbers: CCDC 1848052–1848055, $Nd_3Co_{2.4200(8)}Ge_{6.61(1)}Sn_{0.424(2)}$, $Pr_3Co_{2.3376(5)}Ge_{7.056(7)}$, $Sm_3Co_{2.212(8)}Ge_{6.46(1)}Sn_{0.573(3)}$, and $Pr_3Co_{2.514(5)}Ge_{6.66(7)}Sn_{0.360(2)}$, respectively.

2.3. Physical Properties. Magnetic susceptibility data were collected between 1.8 and 290 K and in magnetic fields up to 9 T, using a Quantum Design Physical Property Measurement System (PPMS). Magnetic susceptibility was also measured in a PPMS under a constant magnetic field of 1000 Oe. Single crystals were zero-field-cooled (ZFC) to 2 K, then magnetic field was applied and susceptibility was measured up to 300 K. The change in magnetization under field, up to 7 T, was measured at a constant temperature of 3 K. The specific heat was measured in the PPMS using a time-relaxation method between 2 and 20 K at zero applied field. The heat capacity of the addenda (background from sample platform and mounting grease) was subtracted from the data as shown in the Supporting Information.

3. RESULTS AND DISCUSSION

3.1. Structures of $Pr_3Co_{2+x}Ge_7$ and $Pr_3Co_{2+x}Ge_{7-y}Sn_y$. $Pr_3Co_{2+x}Ge_7$ and $Pr_3Co_{2+x}Ge_{7-y}Sn_y$ adopt the $La_3Co_2Sn_7$ structure type[7] and are best modeled in the *Cmmm* space group with cell dimensions of $a \sim 4.23$ Å, $b \sim 25.9$ Å, $c \sim 4.27$ Å, and $V \sim 468$ Å.[3] As shown in Figure 1 (left), $Pr_3Co_{2+x}Ge_7$ can be described as an intergrowth of the "$PrGe_3$" ($AuCu_3$-type) with alternating "$PrCoGe_2$" of the $CeNiSi_2$ type along the *b*-direction. The compound consists of distinctive subunits: Pr1@Ge_{12} face-sharing cuboctahedra ($AuCu_3$-type) capped by two Co1 atoms along the axial position and Ge4@Pr_6 trigonal prisms. The Pr2 environment can be described as the part of the "$PrCoGe_2$" structural unit adopting the $CeNiSi_2$ structure type. The Pr1@Ge_{12} cuboctahedron consists of three atomic sites with Co occupying a 4*j* site (labeled as Co1C), with the Pr1–Co1C distance being 3.294(5) Å in $Pr_3Co_{2+x}Ge_7$ and Pr–Ge distance of 3.1–3.2 Å (Table 3), which is in excellent agreement with contacts found in $PrGe_{3.36}$ as prepared by high pressure.[20] The rectangular antiprism has Co1–Ge2, Co1–Ge3, and Co1–Ge4A contacts of 2.344(5) Å, 2.3479(9) Å, and 2.3407(19) Å, respectively, which are also in excellent agreement with the Co–

DOI: 10.1021/acs.cgd.8b00868
Cryst. Growth Des. XXXX, XXX, XXX–XXX

Table 3. Selected Interatomic Distances (Å) for $Pr_3Co_{2+x}Ge_{7-y}Sn_y$

	$Pr_3Co_{2.3376(5)}Ge_{7.056(7)}$	$Pr_3Co_{2.514(5)}Ge_{6.66(7)}Sn_{0.360(2)}$
Pr@[Ge_{12}] cuboctahedron		
Pr1−Ge1A or Sn1A (×4)	3.0060(7)	3.0267(5)
Pr1−Ge1B (×4)	3.101(2)	3.132(1)
Pr1−Co1C (×4)	3.294(5)	3.347(2)
Pr1−Ge2 (×4)	3.184(1)	3.233(1)
Pr1−Ge3 (×4)	3.217(1)	3.217(1)
Ge2−Ge1A/Sn1A	3.168(1)	3.218(1)
Ge3−Ge1A/Sn1A	3.185(1)	3.238(1)
Ge2−Ge1B	2.650(5)	2.668(2)
Ge3−Ge1B	2.670(5)	2.690(2)
Co1C−Ge2	2.344(5)	2.3791(8)
Co1C−Ge3	2.366(5)	2.3566(8)
Co1C−Co1C	2.69(2)	2.86(1)
Co@[Pr_4Ge_4] rectangular antiprism		
Co1−Ge2 (×2)	2.344(5)	2.3791(8)
Co1−Ge3 (×2)	2.3479(9)	2.3566(8)
Co1−Pr2 (×4)	3.3088(8)	3.3277(7)
PrCoGe_2 slab		
Pr2−Ge2 × (2)	3.203(1)	3.209(1)
Pr2−Ge3 × (2)	3.217(1)	3.1756(7)
Pr2−Ge4A (×4)	3.1548(8)	3.175(4)
Pr2−Ge4A (×2)	3.264(1)	3.275(1)
Pr2−Ge4B (×4)	3.09(5)	3.095(4)
Pr2−Ge4B (×2)	3.4(2)	3.51(2)
Ge4A−Ge4A (×2)	2.597(2)	2.612(2)
Ge4A−Ge4B	2.7(1)	2.80(2)

Ge contacts found in isostructural $U_3Co_2Ge_7$, ranging from 2.295(4) to 2.315(2) Å.[21] We also note a slight occupational/positional disorder in the Ge4 site, which is split into two sites Ge4A and Ge4B (occupancy percent ratio of ∼99%:∼1%). Although the occupancy of the Ge4B is small for $Pr_3Co_{2+x}Ge_7$, the occupation of Ge4B systematically increases as a function of lanthanide for the $Ln_3Co_{2+x}Ge_{7-y}Sn_y$ series where the Sm analogue has the highest occupancy (∼10%). This also correlates well with the occupational trend observed with the

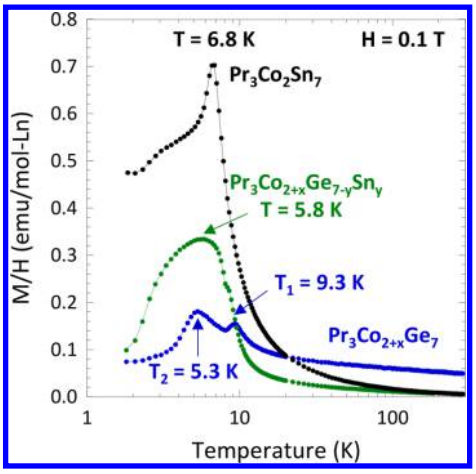

Figure 3. Temperature-dependent magnetization for single crystalline $Pr_3Co_{2.3376(5)}Ge_{7.056(7)}$ ($Pr_3Co_{2+x}Ge_7$), $Pr_3Co_{2.514(5)}Ge_{6.66(7)}Sn_{0.360(2)}$ ($Pr_3Co_{2+x}Ge_{7-x}Sn_x$), and polycrystalline $Pr_3Co_2Sn_7$ measured at 0.1 T. Temperature is in log scale.

systematic decrease in the Co1 occupation (i.e., Sm analogue has Co1 occupancy ∼ 91%). Furthermore, the modeling of the split Ge4 sites into two sites (Ge4A/Ge4B) is similar to the modeling used in the splitting of a Sn site in the related $Eu_2Ni_{1.49(1)}Sn_5$ compound.[22] While the occupancy of Co1 (4*j*) in $Ln_3Co_{2+x}Ge_7$ is close to 90%, the Ni-containing analogues are typically transition metal deficient with a Ni occupancy of 70% in $Pr_3Ni_{2-x}Sn_7$. The occupancies of Co in both the Co1 and Co1C in the germanide analogues also decrease slightly with decreasing Ln covalent radii, though not as much as observed in $Ln_3Ni_{2-x}Sn_7$ (Ln = La−Nd).

3.2. Structural Disorder in the Cuboctahedron. Unlike the cuboctahedra found in $La_3Co_2Sn_7$,[7] the Ge1 site in $Pr_3Co_{2.38}Ge_{7.06}$, or $Pr_3Co_{2+x}Ge_7$ for clarity, exhibits a prolated thermal ellipsoid which is more appropriately modeled as three partially occupied positionally disordered sites to compensate for residual electron density. Furthermore, the distance of 1.347 Å from Ge1A to Co1C is too short to be a reasonable chemically bond, with the Ge1B being approximately halfway in between

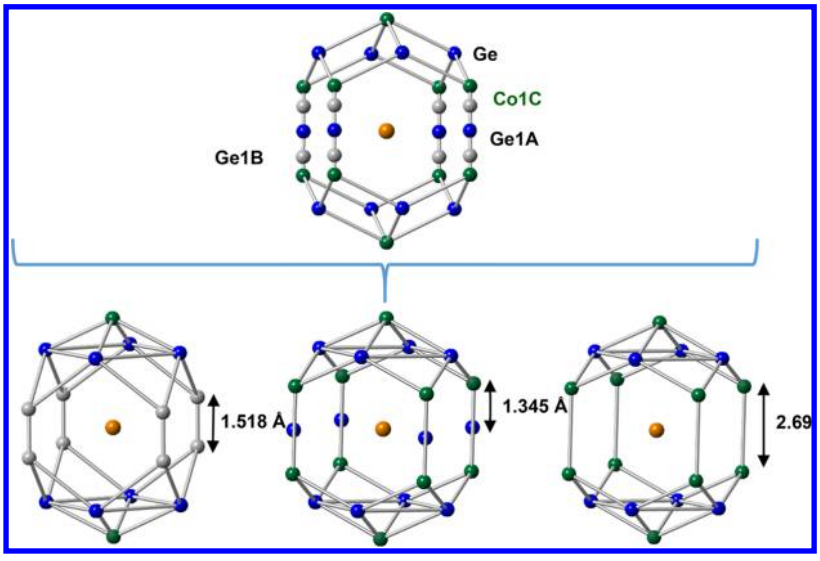

Figure 2. Local chemical environment of Pr1 (orange). Ge1 (blue) is occupationally disordered and leads to Co1C (4*i*) and Ge1B (4*i*), as shown as green and gray spheres, respectively.

DOI: 10.1021/acs.cgd.8b00868
Cryst. Growth Des. XXXX, XXX, XXX−XXX

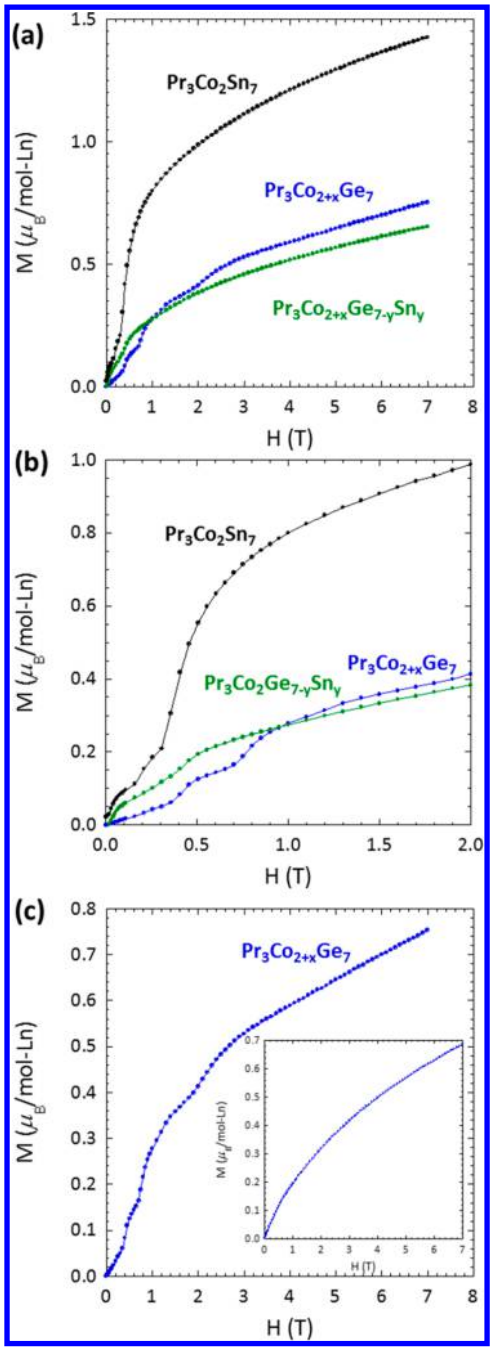

Figure 4. (a). Magnetization under applied field for $Pr_3Co_{2+x}Ge_{7-y}Sn_y$, $Pr_3Co_{2+x}Ge_7$, and $Pr_3Co_2Sn_7$ measured at 3, 4, and 3 K, respectively. (b). Magnetization below H = 2 T shows a close view of the metamagnetic transitions in panel (a). (c) Field-dependent magnetization of $Pr_3Co_{2+x}Ge_7$ at 3 and 8 K (inset) for comparison.

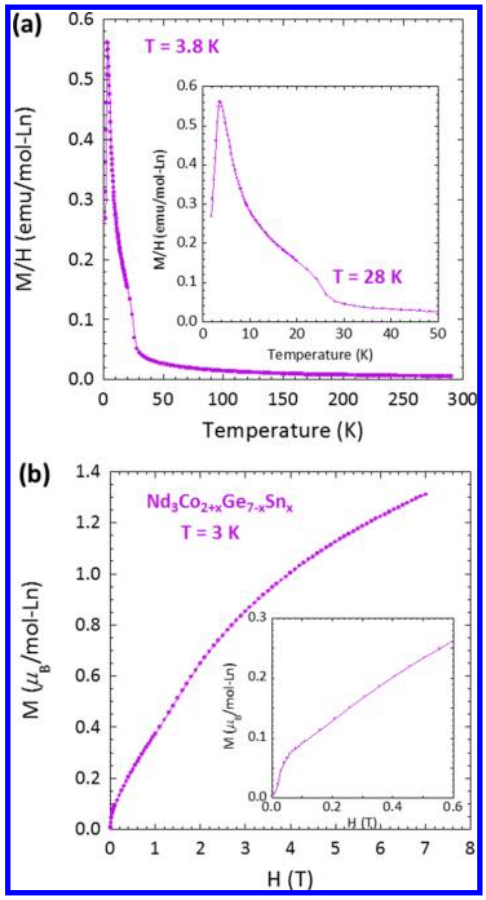

Figure 5. (a). Temperature-dependent and (b) field-dependent magnetization of $Nd_3Co_{2.4200(8)}Ge_{6.61(1)}Sn_{0.424(2)}$ ($Nd_3Co_{2+x}Ge_{7-y}Sn_y$) at 0.1 T and 3 K, respectively. $Nd_3Co_2Ge_{7-x}Sn_x$ has a metamagnetic transition near 0.03 T.

these two atomic sites. Thus, in $Pr_3Co_{2+x}Ge_7$, the Ge1 site is modeled as being split into three crystallographic sites, including the Ge1A (2*a*, *mmm*), Ge1B (4*i*, *m*2*m*), and the Co1C (4*i*, *m*2*m*) Wyckoff sites. The partially occupied split sites were allowed to refine with only the constraints of the sum of the occupancies being equal to unity (necessary for stability of the refinement), and the Co1C−Co1C bond distance of 2.69(2) Å was modeled as a dimer. The resulting occupancies are 54%, 26%, and 20% for Ge1A, Ge1B, and Co1C−Co1C, respectively. It is chemically reasonable for Co to occupy the 4*i* site given the excellent agreement of the Co1C−Ge2 distance of 2.344(5) Å and Co1C−Ge3 distances of 2.366(5) Å with the Co1−Ge2 and Co1−Ge3 distances of 2.344(5) Å (×2) and 2.3479(9) Å (×2) of the cobalt rectangular antiprism. Allowing Co1C to occupy the atomic site as shown in Figures 2 and 3 leads to a more reasonable Co−Co bond distance, given that the Ge−Ge distances are typically at least ∼3.0 Å in a polyhedral environment. Figure 2 shows all the possible occupancy configurations: When Ge1A is occupied, Ge1B and Co1C will not be occupied given the short distances. When Ge1B is occupied, only one of the symmetry related sites will be occupied. When Co1C is occupied, both of the symmetry related sites are occupied and have a contact of 2.69(2) Å, which is within the range of Co−Co distances in germanides found in $Ln_6Co_5Ge_{1+x}Al_{3-x}$ (Ln = Pr, Nd).[23] The occupation of a transition metal on the 4*i* site was also observed in the related compound $Ce_3Ni_{2+x}Si_{8-x}$ ($x \sim 1$), where an elongation of the thermal ellipsoids along the *b*-direction led to the disorder.[11] The result of the Co incorporation forming the cuboctahedron leads to higher transition metal concentration in "$Pr_3Co_{2+x}Ge_7$". For the Sn-flux grown $Pr_3Co_{2+x}Ge_{7-y}Sn_y$, with slightly larger unit cell dimensions ($a \sim 4.26$ Å, $b \sim 26.1$ Å, $c \sim 4.30$ Å, and $V \sim 478$ Å^3), Sn is best occupied at the equatorial position (2*a*) of the cuboctahedron based on the relatively longer bond distances of Sn1A−Ge2 (∼3.22 Å) and Sn1A−Ge3 (∼3.24 Å), compared to the Ge1A and Ge2 (∼3.17 Å) and Ge1A−Ge3 (∼3.19 Å) for $Pr_3Co_{2+x}Ge_7$. Similar to $Pr_3Co_{2+x}Ge_7$, one of the partially occupied sites is also best modeled as Co1C with distances for

DOI: 10.1021/acs.cgd.8b00868
Cryst. Growth Des. XXXX, XXX, XXX−XXX

Co1C−Co1C, Co1C−Ge2, and Co1C−Ge3 of 2.856(10) Å, 2.3791(8) Å, and 2.3566(8) Å, respectively. This observation is also consistent throughout the Nd and Sm analogues. On the basis of the crystallographic data, it is most likely that rare earth Ge polyhedra are stabilized by Sn incorporation, thereby, expanding the polyhedral units. The Co1C at the 4*i* site leads to subsequent higher transition metal occupancy than that observed in $Ln_3Ni_2Sn_7$ (Ln = La−Nd).[10]

3.3. Magnetization. The temperature (T)-dependent magnetization (M) for $Pr_3Co_2Sn_7$, $Pr_3Co_{2+x}Ge_{7-y}Sn_y$, and $Pr_3Co_{2+x}Ge_7$ is shown in Figure 3. $Pr_3Co_2Sn_7$ magnetically orders at T_N = 6.8 K and has an inflection point around 5 K. Below ∼10 K, the susceptibility of $Pr_3Co_{2+x}Ge_{7-y}Sn_y$ increases before a broad transition below 5.8 K. The magnetic susceptibility data were fit using the Curie−Weiss Law: $(C/(T - \theta))$, where C is the Curie constant and θ is the Weiss temperature. The effective magnetic moments of $Pr_3Co_{2+x}Ge_{7-x}Sn_x$ and $Pr_3Co_2Sn_7$ are μ_{eff} = 3.81 μ_B/mol Pr and μ_{eff} = 3.73 μ_B/Pr, respectively. These values are slightly larger than the theoretical moment of Pr^{3+} (3.58 μ_B/Pr), suggesting the possible additional contribution to the magnetic moment from Co. Notably, a large negative Weiss temperature of θ = −53.4(9) K, for $Pr_3Co_{2+x}Ge_{7-y}Sn_y$ indicates the magnetic interaction to be antiferromagnetic and can be attributed to the Pr-triangular lattice while the Sn-only analogue has a negative θ = −3.1(2) K. Interestingly, $Pr_3Co_{2+x}Ge_7$ has two distinctive transitions at 9.3 and 5.3 K, which can also be attributed to each Pr sublattice. Given the similar cell dimension along the *a*- and *c*-directions of $PrCo_{0.85}Ge_2$ of 4.2272(9) Å with $Pr_3Co_{2+x}Ge_7$ with a = 4.2275(14) Å and c = 4.2745(12) Å, the 5.3 K transition can be attributed to the Pr1−Pr1 contacts, which is in the same chemical environment as the $PrCo_{0.85}Ge_2$ of the $CeNiSi_2$ slab. The higher ordering transition found in the $Pr_3Co_{2+x}Ge_7$ at 9.3 K can be attributed to the Pr2−Pr2 contact with a distance of 4.024 Å, which makes up the trigonal prisms, as highlighted in Figure 1 (right). Similar to the $RE_6Co_5Ge_{1+x}Al_{3-x}$,[24] magnetic moments are also higher than the spin-only moments for the Pr analogues. While Co can contribute to the magnetic moment, the small occupancy might not lead to a long-range ordering. For example, $CaCo_2Ge_2$ and the corresponding $BaCo_2Ge_2$ of the $ThCr_2Si_2$ structure type show a ferromagnetic transition below 70 K.[25] The results from the measurement of the specific heat capacity plotted as C/T vs T are shown in the Supporting Information and provide additional evidence of magnetic ordering in $Pr_3Co_{2+x}Ge_7$, and verifies the presence of two magnetic transitions, in agreement with the magnetic susceptibility data.

The field (H)-dependent magnetization at temperatures below the Néel temperature T_N for $Pr_3Co_2Sn_7$, $Pr_3Co_{2+x}Ge_{7-y}Sn_y$, and $Pr_3Co_{2+x}Ge_7$ is shown in Figure 4. $Pr_3Co_{2+x}Ge_7$ exhibits three metamagnetic transitions at 0.46, 0.80, and 2.1 T. When Sn is substituted into the structure, the metamagnetic transitions seem to be suppressed and the remaining transitions occur at lower fields. Both $Pr_3Co_{2+x}Ge_{7-y}Sn_y$ (0.04 and 0.46 T) and $Pr_3Co_2Sn_7$ (0.03 and 0.41 T) have two low field transitions, compared to three metamagnetic transitions in $Pr_3Co_{2+x}Ge_7$.

As the temperature increases to 8 K, the metamagnetic features are suppressed, as shown in Figure 4c. Figure 5 shows the magnetic susceptibility and field-dependent magnetization for $Nd_3Co_{2+x}Ge_{7-y}Sn_y$. With decreasing temperature, the magnetization of $Nd_3Co_{2+x}Ge_{7-y}Sn_y$ shows a transition near 28 K, followed by another antiferromagnetic like transition below 3.8 K, and is presumably due to two rare earth magnetic sublattices. Above 100 K, a Curie−Weiss fit led to an effective moment of μ_{eff} = 3.7 μ_B/mol Nd with Weiss constant of θ = −18.7(3) K, in excellent agreement with the Nd^{3+} spin only moment of 3.62 μ_B. We note the small magnetization for the Sm analogue, and the compound is most likely a temperature-independent paramagnet.

4. CONCLUSION

To study the Ge counterpart of $La_3Co_2Sn_7$, we have grown single crystals of $Pr_3Co_{2+x}Ge_7$ and Sn-substituted compounds $Ln_3Co_{2+x}Ge_{7-y}Sn_y$ (Ln = Pr, Nd, Sm) via In and Sn flux. Structural investigation reveals that the size of the lanthanide has an impact on the structural disorder of the cuboctahedra and Co concentration. Despite the disorder of transition metal and some of the Ge sites, Sn-substitution leads to higher transition metal occupancy by expanding the Pr-Ge polyhedra. We have identified magnetic and multiple metamagnetic transitions similar to those of previously studied Sn compounds, but with transition temperatures higher than the Sn counterparts. Here, all but the Sm compound show Curie−Weiss behavior above the transition temperature, and estimation of the free moment indicates the magnetism, is due to the rare earth element, and we would expect $Ln_3Co_2Ge_7$ to likely host equally complex and rich magnetic properties to those of $Ln_3Co_2Sn_7$.

■ ASSOCIATED CONTENT

Supporting Information

The Supporting Information is available free of charge on the ACS Publications website at DOI: 10.1021/acs.cgd.8b00868.

Atomic positions of $Ln_3Co_{2+x}Ge_{7-y}Sn_y$, heat capacity of $Pr_3Co_2Ge_7$, and elemental analysis (PDF)

Accession Codes

CCDC 1848052−1848055 contain the supplementary crystallographic data for this paper. These data can be obtained free of charge via www.ccdc.cam.ac.uk/data_request/cif, or by emailing data_request@ccdc.cam.ac.uk, or by contacting The Cambridge Crystallographic Data Centre, 12 Union Road, Cambridge CB2 1EZ, UK; fax: +44 1223 336033.

■ AUTHOR INFORMATION

Corresponding Author

*E-mail: Julia.Chan@utdallas.edu.

ORCID

Julia Y. Chan: 0000-0003-4434-2160

Present Address

§Materials Science Division, Argonne National Laboratory, Argonne, IL 60439, USA.

Notes

The authors declare no competing financial interest.

■ ACKNOWLEDGMENTS

J.Y.C. acknowledges the National Science Foundation grant # DMR-1700030 for support of this project. K.A.B. holds an American Fellowship from the American Association of University Women. A.M.P. was part of the UT Dallas − Mexico Summer Research Program sponsored by the U.S. Embassy in Mexico, the National Association of Universities and Higher Education Institutions, and UT Dallas.

■ REFERENCES

(1) Phelan, W. A.; Menard, M. C.; Kangas, M. J.; McCandless, G. T.; Drake, B. L.; Chan, J. Y. Adventures in Crystal Growth: Synthesis and

DOI: 10.1021/acs.cgd.8b00868
Cryst. Growth Des. XXXX, XXX, XXX−XXX

Characterization of Single Crystals of Complex Intermetallic Compounds. *Chem. Mater.* **2012**, *24*, 409−420.
(2) Schmitt, D. C.; Drake, B. L.; McCandless, G. T.; Chan, J. Y. Targeted Crystal Growth of Rare Earth Intermetallics With Synergistic Magnetic and Electrical Properties: Structural Complexity to Simplicity. *Acc. Chem. Res.* **2015**, *48*, 612−618.
(3) Hodeau, J. L.; Chenavas, J.; Marezio, M.; Remeika, J. P. The Crystal Structure of $SnYb_3Rh_4Sn_{12}$ a New Ternary Superconducting Stannide. *Solid State Commun.* **1980**, *36*, 839−845.
(4) Thomas, E. L.; Lee, H. O.; Bankston, A. N.; MaQuilon, S.; Klavins, P.; Moldovan, M.; Young, D. P.; Fisk, Z.; Chan, J. Y. Crystal Growth, Transport, and Magnetic Properties of $Ln_3Co_4Sn_{13}$ (Ln = La, Ce) with a Perovskite-like Structure. *J. Solid State Chem.* **2006**, *179*, 1642−1649.
(5) Rai, B. K.; Oswald, I. W. H.; Wang, J. K. K.; McCandless, G. T.; Chan, J. Y.; Morosan, E. Superconductivity in Single Crystals of $Lu_3T_4Ge_{13-x}$ (T = Co, Rh, Os) and $Y_3T_4Ge_{13-x}$ (T = Ir, Rh, Os). *Chem. Mater.* **2015**, *27*, 2488−2494.
(6) Oswald, I. W. H.; Rai, B. K.; McCandless, G. T.; Morosan, E.; Chan, J. Y. The Proof is in the Powder: Revealing Structural Peculiarities in the $Yb_3Rh_4Sn_{13}$ Structure Type. *CrystEngComm* **2017**, *19*, 3381−3391.
(7) Wolfgang, D.; Schäfer, H. Darstellung und Kristallstruktur von $BaPdSn_3SrPdSn_3$ und $La_3Co_2Sn_7$. *J. Less Common Met.* **1980**, *70*, P1−P10.
(8) Chevalier, B.; Etourneau, J. Antiferromagnetic Properties of the Intermetallics $Ce_3Ni_2X_7$ (X = Ge or Sn). *J. Mater. Chem.* **1999**, *9*, 1789−1792.
(9) Schobinger-Papamantellos, P.; André, G.; Rodríguez-Carvajal, J.; Buschow, K. H. J.; Durivault, L. Magnetic Ordering of $CeNi_{0.78}Sn_2$ and $Ce_3Ni_2Sn_7$ Compounds by Neutron Diffraction. *J. Alloys Compd.* **2001**, *325*, 29−36.
(10) Lin, X.; Bud'ko, S. L.; Thimmaiah, S.; Canfield, P. C. Anisotropic Magnetization, Resistivity and Heat Capacity of Single Crystalline $R_3Ni_{2-x}Sn_7$ (R = La, Ce, Pr and Nd). *J. Magn. Magn. Mater.* **2013**, *331*, 53−61.
(11) Fritsch, V.; Bobev, S.; Thompson, J. D.; Sarrao, J. L. Antiferromagnetic Order in $Ce_3Ni_{2+x}Si_{8-x}$ ($x\approx1$). *J. Alloys Compd.* **2005**, *388*, 28−33.
(12) Chajewski, G.; Pasturel, M.; Pikul, A. P. Magnetic and Related Properties of a Novel Compound $Ce_3Co_2Sn_7$. *J. Alloys Compd.* **2017**, *706*, 244−249.
(13) Schobinger-Papamantellos, P.; André, G.; Rodríguez-Carvajal, J.; Buschow, K. H. J.; Durivault, L. Magnetic Ordering of $CeNi_{0.78}Sn_2$ and $Ce_3Ni_2Sn_7$ Compounds by Neutron Diffraction. *J. Alloys Compd.* **2001**, *325*, 29−36.
(14) Canfield, P. C.; Kong, T.; Kaluarachchi, U. S.; Jo, N. H. Use of Frit-Disc Crucibles for Routine and Exploratory Solution Growth of Single Crystalline Samples. *Philos. Mag.* **2016**, *96*, 84−92.
(15) Thamizhavel, A.; Takeuchi, T.; D Matsuda, T.; Haga, Y.; Sugiyama, K.; Settai, R.; Ōnuki, Y. Unique Magnetic Phases in an Antiferromagnet $CeCoGe_3$. *J. Phys. Soc. Jpn.* **2005**, *74*, 1858−1864.
(16) Kanatzidis, M. G.; Pottgen, R.; Jeitschko, W. The Metal Flux: A Preparative Tool for the Exploration of Intermetallic Compounds. *Angew. Chem., Int. Ed.* **2005**, *44*, 6996−7023.
(17) Krause, L.; Herbst-Irmer, R.; Sheldrick, G. M.; Stalke, D. Comparison of Silver and Molybdenum Microfocus X-ray Sources for Single-Crystal Structure Determination. *J. Appl. Crystallogr.* **2015**, *48*, 3−10.
(18) Sheldrick, G. SHELXT - Integrated Space-Group and Crystal-Structure Determination. *Acta Crystallogr., Sect. A: Found. Adv.* **2015**, *71*, 3−8.
(19) Sheldrick, G. Crystal Structure Refinement with SHELXL. *Acta Crystallogr., Sect. C: Struct. Chem.* **2015**, *71*, 3−8.
(20) Fukuoka, H.; Yoshikawa, M.; Baba, K.; Yamanaka, S. Preparation and Structures of Lanthanoid Germanides, $PrGe_{3.36}NdGe_{3.25}$ and $TmGe_3$ with Double Square Ge-Mesh Structures. *Bull. Chem. Soc. Jpn.* **2010**, *83*, 323−327.
(21) Bobev, S.; Bauer, E. D.; Ronning, F.; Thompson, J. D.; Sarrao, J. L. Synthesis, Structure and Physical Properties of the new Uranium Ternary Phase $U_3Co_2Ge_7$. *J. Solid State Chem.* **2007**, *180*, 2830−2837.
(22) Harmening, T.; Eul, M.; Pottgen, R. Nickel-deficient Stannides $Eu_2N_{i2-x}Sn_5$ - Structure, Magnetic Properties, and Mossbauer Spectroscopic Characterization. *Z. Naturforsch., B: J. Chem. Sci.* **2009**, *64*, 1107−1114.
(23) Zhou, S.; Latturner, S. E. $Nd_8Co_{4-x}Al_xGe_2C_3$: A Case Study in Flux Growth of Lanthanide-Rich Intermetallics. *J. Solid State Chem.* **2016**, *236*, 159−165.
(24) Zhou, S.; Latturner, S. E. Flux Growth and Magnetic Properties of Rare Earth Cobalt Germanide, $RE_6Co_5Ge_{1+x}Al_{3-x}$ (RE = Pr, Nd; $x\approx0.8$). *J. Solid State Chem.* **2016**, *238*, 189−194.
(25) Siggelkow, L.; Hlukhyy, V.; Fässler, T. F. Synthesis, Structure and Chemical Bonding of $CaCo_2Si_2$ and $BaCo_2Ge_2$ − Two New Compounds with $ThCr_2Si_2$ Structure Type. *Z. Anorg. Allg. Chem.* **2010**, *636*, 378−384.

DOI: 10.1021/acs.cgd.8b00868
Cryst. Growth Des. XXXX, XXX, XXX−XXX